A Study of a Weakly Ionized Rotating Plasma

M. M. B. Wijnakker, E. H. A. Granneman and J. Kistemaker
FOM-Institute for Atomic and Molecular Physics, Amsterdam, The Netherlands

Z. Naturforsch. **34a**, 672–690 (1979); received April 19, 1979

Measurements are reported on a weakly ionized rotating argon plasma generated by two identical gas discharges facing each other. In each discharge a current up to 100 A is drawn between a point-like cathode and a ring-shaped anode. Axial magnetic fields up to 0.26 T are applied. All measurements have been done at 1 torr.

For magnetic field strengths below 0.17 T the plasma has a more or less uniform radial distribution; above 0.17 T a contracted plasma column is present along the axis of the cylinder.

In the symmetry plane between the two discharges measurements have been done on the rotational velocity of neutrals and ions, the electron density and temperature, the ion temperature, the plasma potential and the radial pressure distribution. The rotational velocity, the plasma potential and the pressure distribution are also calculated. The theoretical treatment is based on the theory developed by Klüber and Wilhelm and Hong.

In the low magnetic field case velocities of 700 m/sec are found for ions as well as neutrals. The agreement between theory and experiment is good in this case. At high magnetic fields, the ions and neutrals are found to have azimuthal velocities of 1900 and 700 m/sec, respectively.

The radial pressure enhancement due to the centrifugal forces is found to be approximately a factor of two whereas the theory predicts only a factor of 1.2.

In a discharge in which a mixture of argon and xenon is used a relative separation factor of 2.15 is found.

1. Introduction

Since 1965 the possibility of using plasma centrifuges for isotope separation is studied intensively (Bonnevier [1], James and Simpson [2], Nathrath [3], Morozov [4]).

In a plasma centrifuge the ionized particles are set in rotation by means of the Lorentz force. This force is present when an electrical current flows in a direction perpendicular to a magnetic field; it is directed perpendicular to both the magnetic field and the current.

The main advantage of a plasma centrifuge above a mechanical one is the much higher rotational velocities which can be reached and consequently the much higher separative powers which in principle are attainable (Lehnert [5]).

The experiments done so far can roughly be divided into two classes. In the first class one deals with a nearly fully ionized plasma at a relatively low background gas pressure (Boeschoten [6], Bonnevier [1]). In this case very high rotational velocities are possible. However, the electrical power input is large. In the second approach one works with a partially ionized gas. The Lorentz force drives the ions which in their turn drive the neutral particles via collisions. In this situation the rotational velocity may not be as high as in the fully ionized case, however the power is smaller which can possibly lead to an economically more useful device. This is due to the fact that only a small part of the gas has to be ionized. Besides that, according to Lehnert [5] the gas temperature will be lower in the second approach which has a favourable effect on the separative power. In both types of experiments noble gas discharges are used. An appreciable isotope enrichment is measured in the experiments of McClure et al. [7] and James and Simpson [2], Boeschoten [6].

Most theories developed for these systems apply the M.H.D. Equations. Bonnevier [1] developed a theory based on the conservation of momentum for each of the species in the case that the gas is fully ionized. Klüber [8] and Wilhelm and Hong [9] solved the Navier-Stokes equation for D.C. discharges. In both cases the plasma is assumed to be homogeneous and secondary axial and radial mass flows are neglected. Klübers theory predicts plasma potentials which are within a factor of two equal to the measured ones. James and Simpson [10] gave a time-dependent treatment of the Navier-Stokes equation. They find also agreement within a factor of two between the predicted and measured plasma potential.

Reprint requests to Prof. Dr. J. Kistemaker, Fom-Instituut voor Atoom- en Molecuulfysica, Kruislaan 407, Amsterdam, Watergraafsmeer, Niederlande.

0340-4811 / 79 / 0600-0672 $ 01.00/0

In the present experiment we have chosen a weakly ionized gas plasma system. The degree of ionization is of the order of a few percent. It differs from all the other experiments in that a symmetrical arrangement is realized in which a double cathode-anode configuration is used. It is shown that this configuration provides a relatively large region in the device where axial gradients of rotational velocity and plasma potential are small. In this region the rotational velocity, plasma potential and pressure distribution are measured as a function of the radius. In partially ionized systems the mass dependent radial pressure distribution is an important parameter; isotope separation is directly coupled with it.

In Sect. 2 the experimental set up is described.

Because the single-fluid M. H. D.-theory of Klüber and Wilhelm and Hong seems to describe this type of systems very well, we adapt it for our special experimental arrangement. Moreover, in our case also radial ion conduction has to be taken into account. Besides the rotational velocity and the plasma potential, the radial pressure distribution is also calculated (Section 3).

In Sect. 4 the experimental results are shown and a comparison with the theoretical expectations is given.

2. Description of the Experiment

2.1. Apparatus

A schematic view of the cylindrical experiment is given in Figure 1. The length of the device between the two cathodes is 48 cm, the diameter in the region between the anodes 12 cm. The cylinder wall contains 24 electrically insulated cylindrical stainless steel rings, each 2 cm thick. Two of these rings serve as anodes.

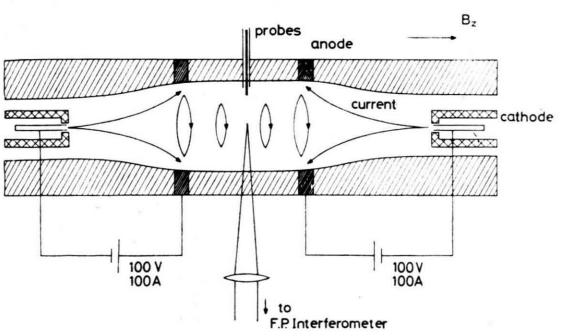

Fig. 1. Schematic view of the experiment. The cylindrical vessel contains two hollow cathodes and two anodes. In the symmetry plane between the two anodes diagnostic ports are present. Along the axis of the cylinder a magnetic field is applied with a strength up to 0.26 T.

The distance between the two anodes is 14 cm. All rings except of course the anode ring are kept electrically floating. The two plasma sources are tantalum hollow cathodes with an inner radius of 0.4 cm. The maximum current which can be drawn is 100 A per source.

Between the two anodes a 5 cm wide floating central ring is located. It contains ports for probe measurements and a (12×0.8 cm) window for optical diagnostics. It allows optical measurements as a function of the full radius. Electrical and pressure probes can be moved radially inwards.

A homogeneous axial magnetic field with a strength up to 0.26 T can be applied externally. This field in combination with the radial component of the electrical current provides the Lorentz force which causes a rotation of the ionized particles in azimuthal direction. Via collisions also the neutral particles are driven in the same direction.

During operation the pressure is kept constant at 1 torr in the volumes behind the hollow cathodes.

2.2. Diagnostic Techniques

Most of the measurements are performed as a function of the radius in the symmetry plane between the two anodes.

A pressure scanned Fabry-Perot interferometer with sufficient wavelength resolution is used to determine the rotational velocity of ions and neutrals from the Doppler shift of spectral lines of the light emitted by the plasma particles.

The temperature of neutrals and ions can be calculated from the Doppler width of spectral lines. Extra broadening due to Zeeman splitting is avoided by inserting a polarization filter in the light path.

Near the wall the temperature is determined by means of a W-Rh thermocouple with a tiplength of 1 mm and a diameter of 0.2 mm. The electron (ion) density as a function of the radius is determined by adding a small amount of hydrogen to the discharge and measuring the Stark broadened H_β line.

The intensity of some spectral lines of the argon discharge is registered as a function of the radius by means of a 0.5 m Jarrel-Ash monochromator.

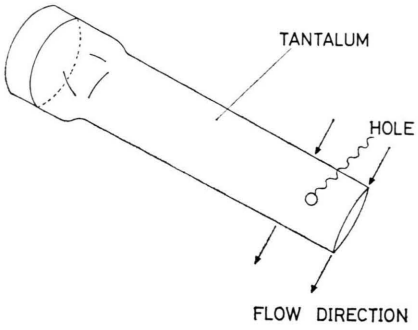

Fig. 2. Biconvex pressure probe for measuring the static pressure. The dimensions in the directions along and perpendicular to the flow are approximately 4 and 1 mm, respectively.

This gives an impression of the radial distribution of the ion and neutral density.

The electron temperature is measured in two ways: First of all the intensities of various neutral argon lines are measured. From the relative intensities a so-called Boltzmann plot can be constructed (McWhirter [11]) which gives, under assumption of PLTE, the electron temperature.

In the region near the wall the electron temperature is also measured with a probe. For this a floating double probe is used. The tip length is 1.5 mm; the diameter 0.2 mm. The electron temperature follows directly from the slope of the current-voltage characteristic (Chen [12]). In the region near the wall the plasma potential as a function of the radius is measured with a doubly shielded floating Langmuir probe. It has a tungsten tip with a length of 1.0 mm and a diameter of 0.2 mm.

The static pressure is measured as a function of the radius by means of a hollow biconvex tantalum pressure probe with a height of 4 mm and a width of 1 mm (see Figure 2). 5 millimeter from the tip a hole with a diameter of 0.5 mm connects the experiment with a capacitive pressure meter (MKS 145 BHS-100). This probe has been tested in a windtunnel for velocities below and above Mach 1. The same kind of probe is also used to analyze the composition of gasmixtures in case more than one gas is present in the device. A small amount of gas then flows through the probe to a mass spectrometer (Micromass). Because there is a permanent flow the diameter of the hole in the probe has to be much smaller. A diameter of 0.1 mm is chosen for these measurements.

3. Theoretical Analysis

The theoretical treatment of the gas-plasma system presented in this paper will be closely related to those given by Klüber [8] and Wilhelm and Hong [9]. For convenience where possible, the nomenclature is chosen identical to that used by Wilhelm and Hong [9], hereafter being called W & H.

The analysis is applied for the simplified set up given in Figure 3 (compare with Figure 1). The total length of the cylindrical vessel is equal to $2c$, the radius is R_0. In each end wall of the cylinder a circular cathode with radius R_1 is present. The cylinder wall contains two circular anodes at distances c_0 from the central plane of the cylinder. The cathode and anode rings are assumed to be infinitely thin. In Fig. 3 a possible current path is shown. We assume the presence of a homogeneous magnetic field B_0 in axial (z) direction which is much larger than any of the magnetic fields induced by the discharge currents; consequently azimuthal (θ) and radial (r) magnetic fields are neglected.

The azimuthal component of the $\boldsymbol{j} \times \boldsymbol{B}$ force ($j_r B_0$) sets the plasma in a rotational motion. This rotational motion causes a centrifugal force which, as we will show, can lead to wall pressures appreciably higher than those on the axis of the system.

The flow in the system is assumed to be purely azimuthal i.e. secondary flows in radial and/or axial direction are neglected. This means that the plasma behaves as an incompressible fluid ($\nabla \cdot \boldsymbol{v} = 0$) and that density gradients $\nabla \varrho$ (pressure gradients ∇p) are only present in radial direction. We shall see later that this can only be true in a limited part of the cylinder.

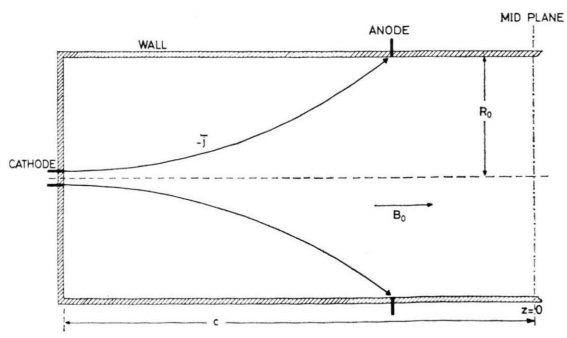

Fig. 3. Simplified scheme of the discharge used in the theoretical model. $z = 0$ is the symmetry plane of the device. A possible current path j is shown. The distance between the mid plane and the cathode is c, the radius of the cylinder R_0.

The plasma is characterized by the following parameters: an electrical conductivity along the magnetic field σ; an electrical conductivity perpendicular to the magnetic field in radial direction $\sigma_\perp$; a "Hall" electrical conductivity in azimuthal direction σ_H; an isotropic viscosity μ and electron and ion collision frequencies ν_e and ν_i. The plasma is assumed to be homogeneous, which means that all these parameters have to be independent of the spatial coordinates, i.e. the formalism is only valid as long as the radial pressure gradients are small. We will show in Sect. 4 that this is at least partly the case under certain experimental conditions. With the above mentioned quantities a number of non-dimensional parameters can be defined: the Hartmann number H which is a measure of the strength of the Lorentz force relative to the viscous force:

$$H = (\sigma/\mu)^{1/2} B_0 R_0 \tag{1}$$

and the electron and ion Hall parameters β_e and β_i:

$$\beta_e = \omega_e/\nu_e; \quad \beta_i = \omega_i/\nu_i \tag{2}$$

in which ω_e and ω_i are the electron and ion gyro frequencies.

In the magnetogasdynamic approximation the equation of conservation of electric charge density ($\nabla \cdot \boldsymbol{j} = 0$) and the Navier-Stokes equation both combined with the generalized Ohm's law give rise to the following set of differential equations:

$$\frac{1}{r}\frac{\partial}{\partial r}\left(r\frac{\partial \varphi}{\partial r}\right) + \frac{\sigma}{\sigma_\perp}\frac{\partial^2 \varphi}{\partial z^2} - B_0 \frac{1}{r}\frac{\partial}{\partial r}(r v_\theta) = 0\,, \tag{3a}$$

$$\mu\left[\frac{\partial}{\partial r}\left(\frac{1}{r}\frac{\partial}{\partial r}(r v_\theta)\right) + \frac{\partial^2 v_\theta}{\partial z^2}\right] - \sigma_\perp B_0\left(-\frac{\partial \varphi}{\partial r} + v_\theta B_0\right) = 0\,, \tag{3b}$$

$$\frac{\partial p}{\partial r} = \varrho \frac{v_\theta^2}{r} - \sigma_H B_0\left(-\frac{\partial \varphi}{\partial r} + v_\theta B_0\right), \tag{3c}$$

$$\frac{\partial p}{\partial z} = j_r B_\theta - j_\theta B_r = 0\,. \tag{3d}$$

In these equations φ and v_θ are the potential and the azimuthal velocity, respectively; p and ϱ stand for the pressure and the density, p and ϱ being related via:

$$p/\varrho = kT/m \tag{4}$$

in which T is the temperature, k the Boltzmann constant and m the mass of the particles. Equations (3c) and (4) give

$$\frac{\partial p}{\partial r} = \frac{m}{kT}\frac{v_\theta^2}{r} p - \sigma_H B_0\left(-\frac{\partial \varphi}{\partial r} + v_\theta B_0\right). \tag{5}$$

In principle the temperature can be found via the energy equation; however, we will insert experimentally determined temperature values.

Before solving the set of equations (see Appendix) we first make a few general remarks. Equations (3a) and (3b) fully determine the potential φ and the rotational velocity v_θ as functions of z and r. W & H show that in case σ, $\sigma_\perp$ and σ_H are determined only by electron conduction (i.e. $\beta_e \gtrsim 1$; $\beta_i \ll 1$) solutions for φ and v_θ can be expressed in terms of the Hartmann number H and the electron Hall parameter β_e. In that case the electrical conductivities can be written as:

$$\sigma_\perp = \frac{1}{1+\beta_e^2}\sigma; \quad \sigma_H = \frac{\beta_e}{1+\beta_e^2}\sigma\,. \tag{6}$$

However, in the present experimental situation the plasma is only weakly ionized. It will be shown that the ion-Hall parameter in this case in at least part of the cylinder is of the order of unity which means that the ion conduction can be important in that part and has to be included. Mitchner and Kruger [13] give the following modified expressions for $\sigma_\perp$ and σ_H in case the conduction is due to both electron and ion drifts:

$$\sigma_\perp = \frac{(1+s)}{(1+s)^2+\beta_e^2}\sigma; \quad \sigma_H = \frac{\beta_e}{(1+s)^2+\beta_e^2}\sigma \tag{7}$$

in which s is the so-called ion-slip factor:

$$s = \left(\frac{\varrho_n}{\varrho_n + \varrho_i}\right)^2 \beta_e \beta_i\,. \tag{8}$$

ϱ_n and ϱ_i are the neutral particle and ion densities respectively. A value $s > 1$ implies that the major part of the radial current is carried by the ions. Note that the expression for $\sigma_\perp$ in Eq. (7) reduces to that for $\sigma_\perp$ in (6) provided that in (6) β_e is replaced by an effective Hall-parameter β_{eff}, equal to:

$$\beta_{eff} = \left[\frac{s(1+s)+\beta_e^2}{(1+s)}\right]^{1/2}. \tag{9}$$

In cases where the ion conduction is important this means that the ions can have non negligible

radial drift velocities inwards. This can lead to a radial fluid velocity (in this one-fluid model being the weighted average of the radial ion, electron and neutral particle velocities) no longer negligible in comparison with the rotational velocities. Janssen et al. [14] showed that for plasmas with an appreciable degree of ionization the radial fluid velocities have to be taken into account. However in the present experiment the degree of ionization is of the order of a few percent which means that the ions have a small weight in the total fluid velocity. Besides that in the regions in the experiment where the ion conduction is found to be important (the central region, see Sect. 4), the radial currents are relatively small and consequently the ion drift velocity will also be small.

Because the azimuthal velocity v_θ and the potential φ are functions of z and r, Eq. (3c) shows that

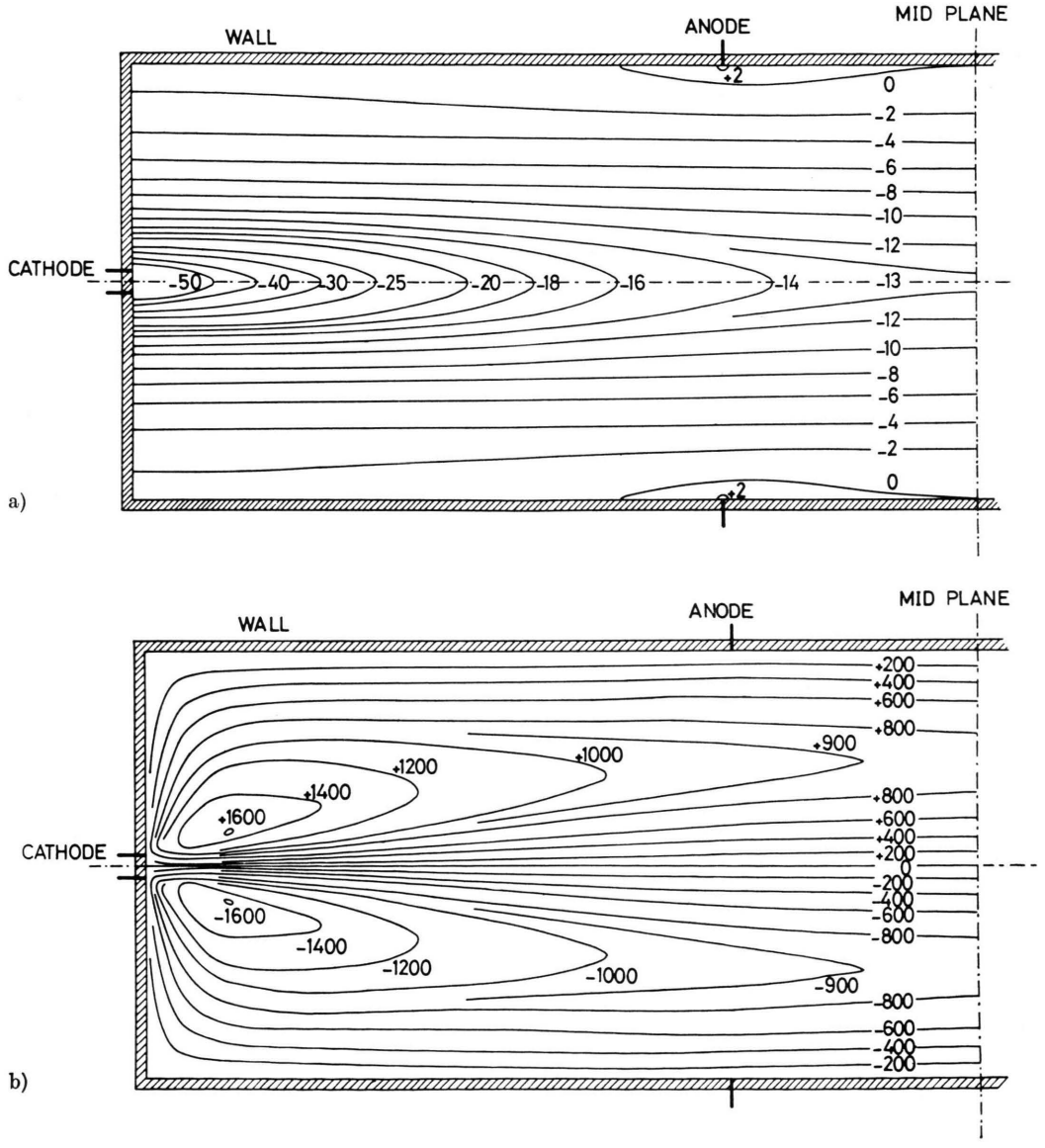

Fig. 4. Potential distribution (a) and azimuthal velocity distribution (b) in one half of the (symmetrical) experiment. The parameters used in this calculation are: $c/R_0 = 4$, parallel conductivity $\sigma = 700\ \Omega^{-1}\ \mathrm{m}^{-1}$, Hartmann number $H = 25$ and effective Hall parameter $\beta_{\mathrm{eff}} = 8$ (see text).

also $\partial p/\partial r$ and consequently p will be a function of z. This is in conflict with Eq. (3d) which, if one assumes B_θ and B_r to be zero, clearly states that p is not z-dependent. So the formalism is only valid under conditions in which v_θ and φ (or better $\partial\varphi/\partial r$) are slowly varying functions of z. The experiment described in Sect. 2 was designed to provide this feature in a large part of the plasma system (see Figure 4). However, because there is a positive radial pressure gradient in the mid-section of the device and a radial pressure gradient equal to zero at the end walls, $z = \pm c$, there is bound to be a pressure gradient in axial direction which will cause a secundary flow. This secundary flow will limit the radial pressure gradients built up by the centrifugal forces. Note that in the mid-section the direction of this flow is radially outwards, i.e. opposed to the radial ion drift mentioned before. The extent to which the assumption that the radial fluid velocity is small compared to the azimuthal velocity is valid, will have to be justified by the experimental results.

The solution of the set of Eqs. (3a), (3b) goes along the lines given by W & H. The boundary conditions for this case are the following: The velocity v_θ has to be zero at the walls i.e.:

$$v_\theta(r, z) = 0 \quad \text{for} \quad z = \pm c \quad \text{and} \quad r = R_0 . \tag{10}$$

The current density is assumed to be zero everywhere on the walls except of course at the position of the cathodes and the anodes. This is expressed by using delta-function type boundary conditions:

$$-\sigma\left(\frac{\partial\varphi(r,z)}{\partial z}\right) = I\frac{\delta(r - R_1)}{2\pi r} \quad \text{at} \quad z = \pm c; \tag{11a}$$

i.e.
$$-\sigma\int_0^{R_0}\frac{\partial\varphi(r,z)}{z}\cdot 2\pi r\,\mathrm{d}r = I ,$$

$$-\sigma_\perp\left(\frac{\partial\varphi(r,z)}{\partial r}\right) = I\frac{\delta(z \pm c_0)}{2\pi R_0} \quad \text{at} \quad r = R_0 . \tag{11b}$$

In these expressions I is the total current. Note that in view of the experimental situation sketched in Sect. 2 no constraints have to be imposed on the potential at the walls.

Although the geometrical shape of the vessel and the arrangement of cathodes and anodes leading to this set of boundary conditions makes the solution of these equations more complicated than in the case of W & H, the procedure is in principle straightforward. It leads to an analytical solution in which φ and v_θ are expressed in terms of an infinite series of zeroth and first order Bessel functions, respectively. Because it contains rather lengthy expressions the reader is referred to the appendix for the actual solution of the problem. Here it suffices to show some of the results. Figures 4a and b show the solution for the potential and the azimuthal velocity, respectively, for a typical case.

Note that between the two anode rings the potential and the velocity are nearly independent of z. This holds for most of the experimental conditions.

Because most measurements are concerned with the symmetry plane ($z = 0$) we will now concentrate on this plane. From the model a few conclusions can be drawn with regard to the azimuthal velocity. In Fig. 5 we have plotted the non-dimensional quantity $(\mu/IB_0)\, v_{\max}(z = 0)$ as a function of the Hartmann-number H for various values

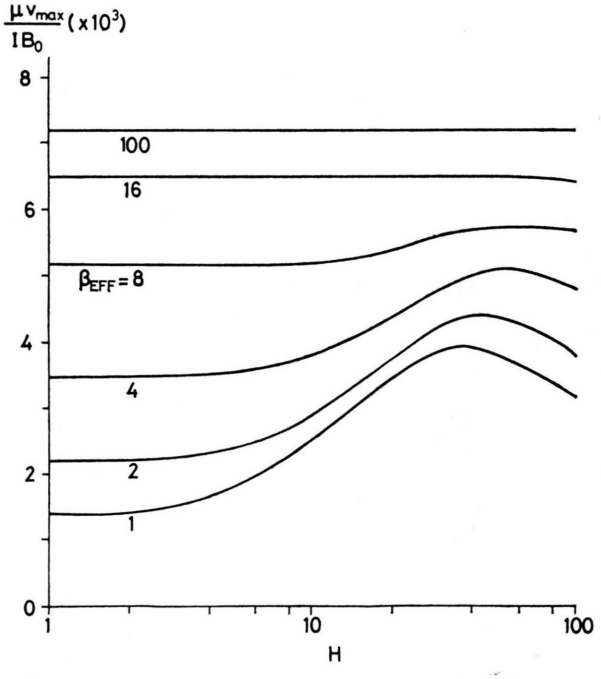

Fig. 5. The maximum azimuthal velocity (multiplied by μ/IB_0; μ = coefficient of viscosity, I = arc current, B_0 = magnetic field) for different values of the effective Hall parameter β_{eff} as a function of the Hartmann number H, $c/R_0 = N = 4$ is kept constant. In those cases where the curves are (nearly) horizontal, the rotational velocity is no longer a function of the conductivity σ if μ/IB is a constant. Note that $H = (\sigma/\mu)^{1/2} B_0 R_0$.

of the effective Hall-parameter β_{eff}, $v_{\max}(z=0)$ being the maximum value of the v_θ-velocity in the plane $z=0$. The position of this maximum velocity is located roughly halfway between the axis and the wall of the cylinder. This radial position is only very weakly dependent on H and β_{eff}. From Fig. 5 it can be seen that for a given value of the viscosity μ, the discharge current I and the magnetic field strength B, this maximum velocity will only be weakly dependent on β_{eff} and H; in the parameter region $1 \leqq H \leqq 100$ and $4 \leqq \beta_{\text{eff}} \leqq 100$, $(\mu/IB_0)v_{\max}$ $(z=0)$ varies no more than a factor two. Provided μ, I and B_0 are accurately known, a rough knowledge of β_{eff} and H suffices to determine the azimuthal velocity in the mid plane. We will come back to this in the next section.

4. Results

In this chapter we will give results obtained in an argon discharge. First the character of the discharge will be described and measurements on neutral particle (and ion) temperature, electron temperature and electron density will be given. Subsequently measurements on the plasma potential and the rotational velocities of the argon atoms and ions will be presented and compared with theoretical values. Finally the measured pressure distribution will be compared with the theoretically predicted one. All these measurements are done in the mid-plane.

The optical measurements are given as a function of radius. This is not completely correct because the necessary Abel transformation has not been applied. We will come back to this point later. Table 1 gives a survey of the values of the characteristic plasma parameters at the centre of the vessel and at 1 cm from the cylinder wall for each of the two discharge modes (see Section 4.1).

4.1. The Discharge

All measurements are done at a filling pressure of 1 torr. During the measurements this pressure is kept constant in the volumes behind the two

Table 1. Values of the basic plasma parameters at a filling pressure of 1.0 torr argon.

Discharge mode		Diffuse	Contracted	r (cm)	Unit
Magnetic field strength		0.13	0.26		T
Arc current		100	100		A
Arc voltage	(1)	58.0 ± 0.5	83.0 ± 0.5		V
Arc voltage corrected	(1)	18.5 ± 2.0	38.0 ± 2.0		V
Ion (electron) density		8.0 ± 2	49 ± 25	0	$\times 10^{18}$ m^{-3}
		22 ± 2	1.3 ± 0.6	5	$\times 10^{18}$ m^{-3}
Heavy particle temperature		5950 ± 1300	9700 ± 2500	0	K
		1800 ± 400	2750 ± 500	5	K
Electron temperature	(2)	8100 ± 2300		0	K
	(2)	8100 ± 2300		5	K
	(3)	11600 ± 2300	46400 ± 5800	5	K
Neutral density	(4)	4.3 ± 1.0	3.5 ± 0.9	0	$\times 10^{20}$ m^{-3}
		45 ± 6	8.8 ± 1.4	5	$\times 10^{20}$ m^{-3}
Rotational velocity (max)					
ions		750 ± 75	1850 ± 75		m s^{-1}
neutrals		700 ± 100	750 ± 150		m s^{-1}
Degree of ionization		1.3 ± 0.2	12 ± 10	0	%

(1) arc-voltage and corrected arc-voltage are the voltages with cathode and anode falls included and excluded, respectively.
(2) electron temperature determined from the relative intensity of Ar I lines.
(3) electron temperature obtained from probe measurements.
(4) calculated neutral density assuming the pressure in the centre to be 0.4 torr.

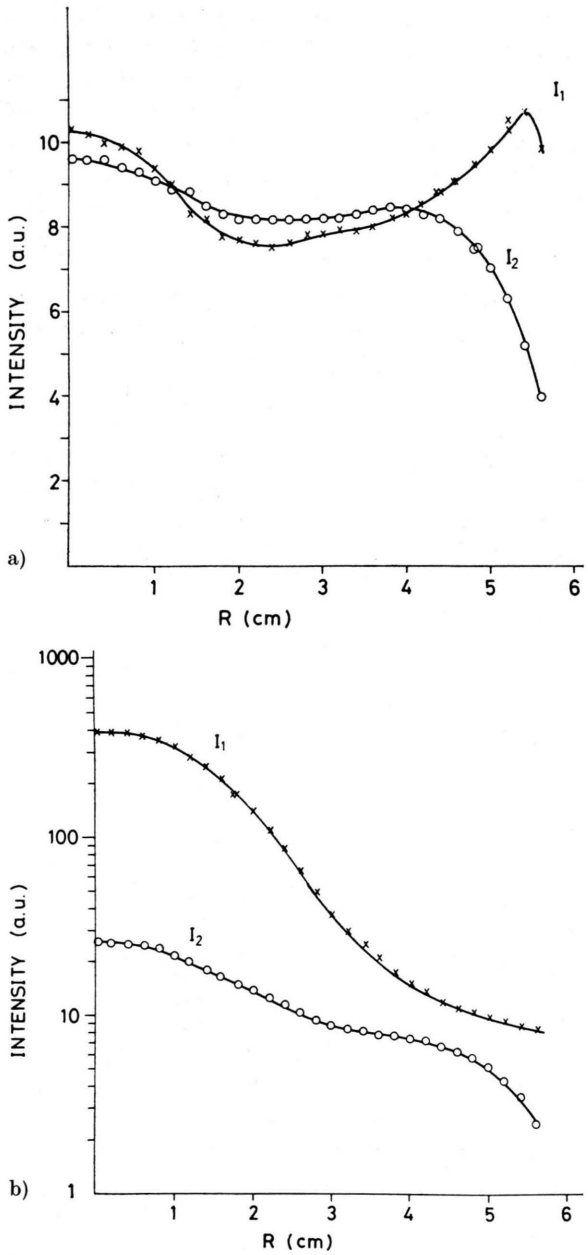

Fig. 6. Intensity of the 4702 Å neutral and 4806 Å ion spectral lines as a function of the radius in the diffuse (a) and the contracted mode (b). The current is 100 A, and the filling pressure is 1 torr. Note the logarithmic scale in Figure b. I_1 = ion line, I_2 = neutral line, $B = 0.13$ T (a); $B = 0.26$ T (b).

cathodes. At this pressure two distinctly different discharge modes can exist: at low values of the magnetic field strength ($\leqq 0.17$ T) the discharge fills the vessel more or less uniformly. It radiates bright "white" light at all radii. At approximately 0.17 T the discharge abruptly changes character. It now shows a small blue core surrounded by a mantle which radiates much less. The diameter of this core is approximately 3 cm. The blue color is characteristic for radiation of ionized argon. In the following these two modes will be denoted as the diffuse and the contracted mode, respectively. We will not discuss the physical mechanisms causing this change here. Possible explanations are given by Gerasimov [15], Ulyanov [16] and Baranov [17].

In Fig. 6a and 6b for both types of discharges the intensities of atomic and ionic spectral lines are shown as a function of radius. It confirms that in the diffuse mode the plasma fills the cylinder more or less homogeneously. The ion and neutral intensities do not vary much over the radius. In reality the radial dependence is stronger than given in Figure 6 because no Abel transformation is applied. In the contracted mode the intensities of similar lines decrease steeply from the centre to the wall (Fig. 6b, note the logarithmic scale).

4.2. Heavy Particle Temperature

The heavy particle temperature is determined in the following way (see Figure 7). Near the wall it is measured by means of a W-Rh thermocouple. The measured temperature is corrected for the extra amount of heat transferred to the thermocouple due to the rotational velocity of the gas and for losses due to radiation and conduction. In the centre the temperature is determined from the Doppler halfwidth of the argon ion 4806 Å line (Wiese [18]). In a rotating plasma this procedure only yields accurate temperatures in the centre of the column. For any point outside the centre the unavoidable integration over the optical line of sight not only means averaging over points with different Doppler widths, but also with different Doppler shifts. This may cause errors up to a factor of two (Kress [19]). Figure 7 shows that the temperature in the contracted mode is considerably higher than in the diffuse one.

4.3. Electron Temperature

The electron temperature is determined in two ways. From the centre of the column to approximately 1 cm from the wall the relative intensities of various spectral lines of the argon neutral 3p, 4s,

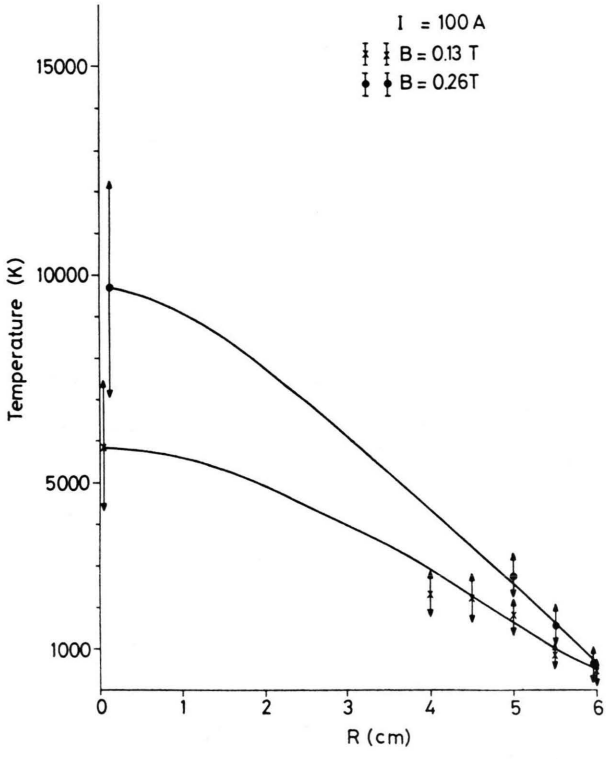

Fig. 7. Heavy particle temperature as a function of the radius for magnetic field strengths of 0.13 and 0.26 T. The temperature at $R=0$ cm is deduced from the Doppler width of the argon-ion 4806 Å line. Close to the wall the temperature is measured by means of a thermocouple. The current is 100 A and the filling pressure is 1 torr. The part of the curves between $R=0$ and $R=4(5)$ cm is interpolated.

5d, 5s system are measured. Via a Boltzmann plot the electron temperature can be deduced from this (McWhirter [11]). This temperature is found to be nearly constant with radius for the diffuse ($T_e = 0.7 \pm 0.2$ eV) as well as for the contracted mode ($T_e = 1.2 \pm 0.4$ eV). However, there is evidence that the values determined in this way are probably too low because the required partial local thermodynamic equilibrium (PLTE) may not be achieved at these densities (Pots et al. [20]). Therefore near the wall (0.5—1.5 cm) the electron temperature is also determined by means of an electric double probe (Chen [12]). This yields temperatures (again constant with radius) of 1.0 ± 0.2 eV and 4.0 ± 0.5 eV for both modes, respectively. These latter values we assume to be more realistic values for the mid plane. Because we do not know to what extent these numbers are characteristic for the whole vessel we apply in the further calculations two sets of electron temperatures for both discharge modes: 1.0 and 2.5 eV for the diffuse and 1.2 and 4.0 eV for the contracted mode, respectively. The value of 2.5 eV is chosen because these types of discharges tend to have average electron temperatures higher than the 1 eV measured in the mid-plane (Pots et al. [20]).

4.4. Ion (Electron) Density

The radial dependence of the ion density is determined from the Stark-broadening of the hydrogen Balmer H_β line (4861 Å). For this purpose a small amount ($\approx 3\%$) of hydrogen is added to the discharge. In the contracted mode this procedure causes problems because even a small amount of hydrogen changes the character of the discharge noticeably. Therefore the amount of hydrogen which could be added to the discharge without

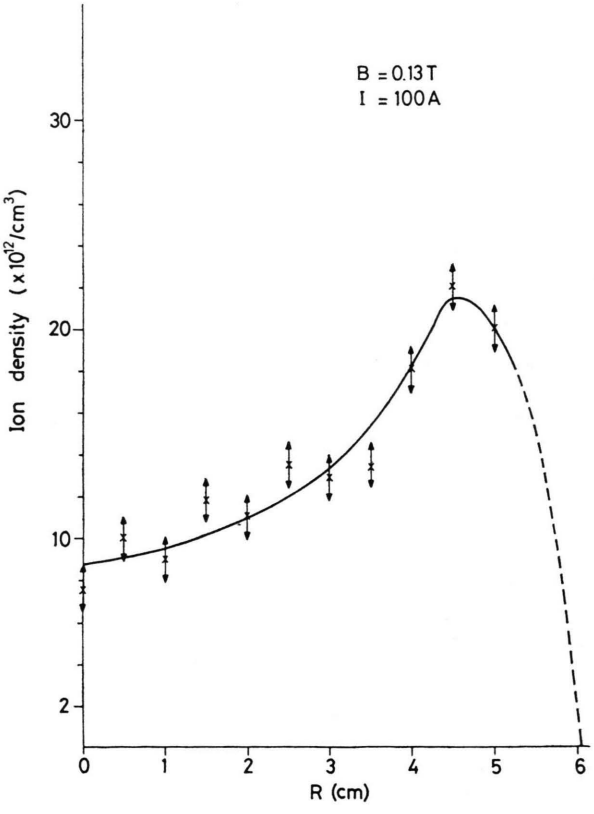

Fig. 8. Ion density as a function of the radius for a magnetic field strength of 0.13 T (diffuse mode). This density is deduced from the Stark broadening of the hydrogen Balmer β line (4861 Å). The current is 100 A. The filling pressure is 1 torr. The temperature profile given in Fig. 7 is used for the calculation of the density.

changing it, is such that only in the centre of the column a reliable Stark profile can be measured (see Table 1). In Fig. 8 the ion density is given as a function of radius for the diffuse mode. In deducing the Doppler part of the line the (partly interpolated) temperature profile of Fig. 7 is used (Davies and Vaughan [21]). Because the rotational velocity of the hydrogen atoms is approximately equal to that of the argon atoms, the combined Stark and Doppler widths are much larger than the Doppler shifts caused by the rotation and therefore errors due to integration over points with different Doppler shifts are considered to be small.

The intensity of the ion spectral like shown in Fig. 6a rises near the centre of the cylinder; the ion density profile (Fig. 8) does not show this feature. Because the intensity of a spectral line is a rather strong function of the electron temperature, this suggests that the electron temperature at the centre of the discharge is slightly higher than near the wall. Note that for the diffuse mode the ion pressure $n_i kT_i$ is only very slowly varying with radius.

4.5. Rotational Velocity

For both modes the azimuthal velocity of the argon neutral atoms and ions are determined as a function of radius (see Figure 9 and 10). Because one integrates along the line of sight the measured velocities usually are too low. A calculation of Kress [19] shows that this amounts to a maximum error of approximately 20%. In the diffuse mode the neutrals have a maximum velocity of 700 m/sec at a position about 3.5 cm from the axis of the discharge. The ions have about the same velocity, however, the maximum is shifted towards the centre ($r = 2$ cm). In the outside regions the neutrals have a higher rotational velocity than the ions, therefore it is improbable that in the mid plane the neutrals are driven by the ions. Possibly, via viscous forces the neutrals in the mid plane are driven by the rotating gas (plasma) in the anode plane, where the $\boldsymbol{j} \times \boldsymbol{B}$ forces are stronger than in the mid plane. It is not understood so far why in the outside regions of the mid plane the ions have a lower velocity than the neutrals.

In the contracted discharge the ions obtain a maximum velocity of 1900 m/sec at a position about 2 cm from the axis (see Figure 10). There is an appreciable velocity slip between ions and neutral particles. The neutrals have a much lower velocity and no sharp maximum.

Before comparing the experimental results on the velocities given in Figs. 9 and 10 with predictions from the theory developed in Sect. 3 we first make the following general remarks: because the theory requires a homogeneous plasma as far as the conductivities and the viscosity are concerned we have to analyze to what extent this is true in the present experiment. We consider the diffuse mode first: Because the plasma is weakly ionized, in first approximation the coefficient of viscosity μ is determined by the viscosity of the neutral particles, which is not a function of the particle density. It is

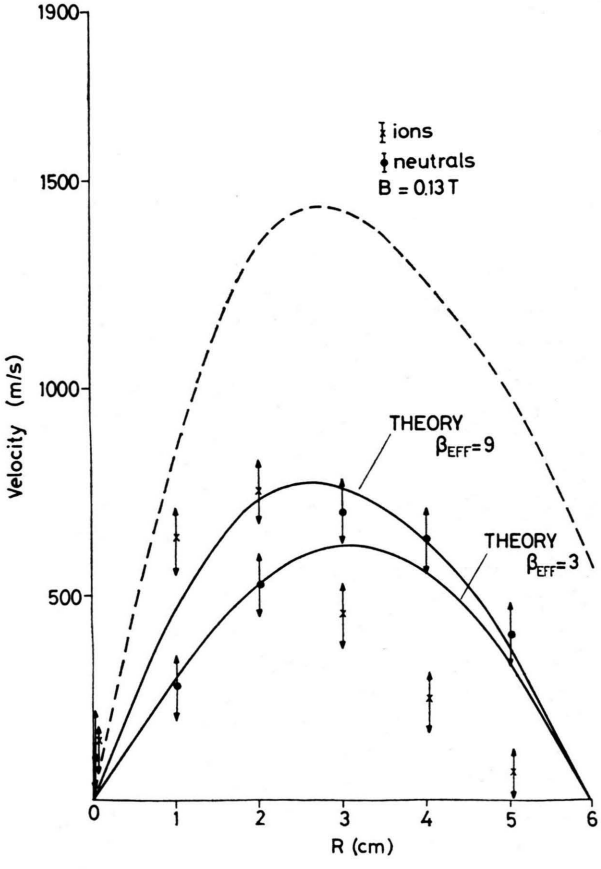

Fig. 9. Azimuthal velocity of ions and neutrals as a function of the radius at a magnetic field strength of 0.13 T (diffuse mode). The arc current is 100 A; the filling pressure is 1 torr. The solid lines are theoretical curves for two values of the effective Hall parameter ($\beta_{eff} = 3$ and 9). The dots and crosses are measured points. The dashed curve gives the theoretical velocity profile required to match the theoretical and measured radial pressure distribution (see Fig. 13).

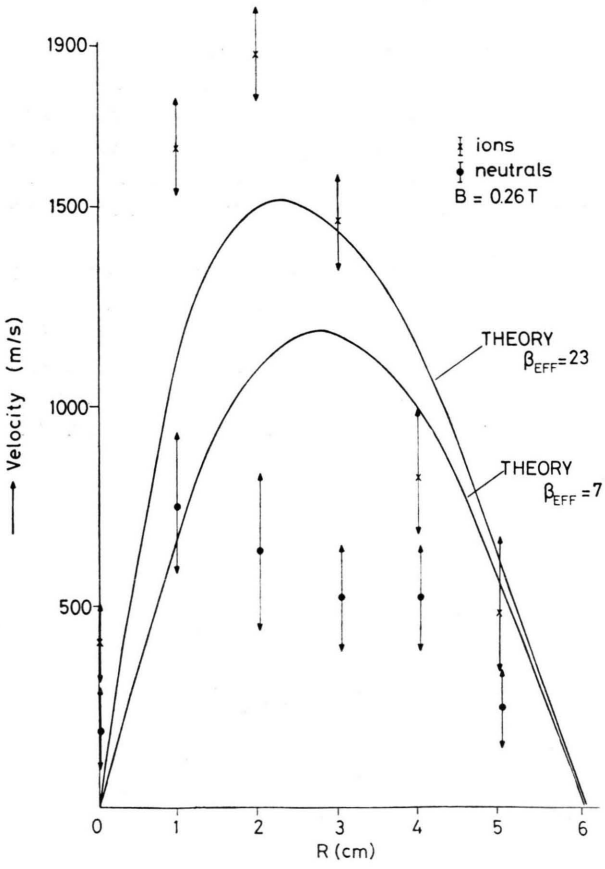

Fig. 10. Azimuthal velocity of ions and neutrals as a function of the radius at a magnetic field strength of 0.26 T (contracted mode). The arc current is 100 A, the filling pressure 1 torr. The two solid lines denoted by $\beta_{\text{eff}} = 7$ and 23 are the theoretical curves. Note that the ions have a much higher velocity than the neutrals.

only a function of temperature ($\mu \propto T^{1/2}$). Figure 7 shows that for the diffuse mode the temperature in the mid-plane varies approximately a factor of 10 with radius i.e. μ varies a factor 3.

Although the degree of ionization is low (1—2%) the parallel conductivity (σ) is still mainly determined by the Spitzer conductivity (electron-ion collisions [13] and is therefore only a function of the electron temperature ($\sigma \propto T_e^{-3/2}$). T_e varies probably less than a factor of two. The perpendicular conductivity ($\sigma_\perp$), however, depends on the parallel conductivity and the effective Hall parameter β_{eff}, which contains β_e and β_i (Equations 8 and 9). β_e and β_i are inversely proportional to the electron and ion collision frequencies ν_e and ν_i [Equation (2)]. For our conditions ν_e is equal to the Spitzer collision frequency [13] which is proportional to $n_i T_e^{-3/2}$. The ion density n_i varies a factor 2—3 with radius (see Figure 8). ν_i is the ion-neutral collision frequency which is equal to $n_n \bar{g}_{in} \bar{Q}_{in}$ [13]. The neutral density n_n varies a factor 10 with radius (see Table 1), the ion-neutral relative mean speed $\bar{g}_{in}$ varies with $T^{1/2}$ (heavy particle temperature). T also varies approximately a factor 10 with radius. Because the average ion-neutral collision cross-section $\bar{Q}_{in}$ is very weakly dependent on the particle temperature [24], ν_i varies roughly a factor 3 with radius. In conclusion in the mid-plane the parameters μ, σ and $\sigma_\perp$ vary probably no more than a factor 3 with radius. The situation is completely different in the contracted discharge; the plasma is certainly not homogeneous (see Figure 6b and 7). So in comparing theory with experiment we will concentrate on the diffuse mode.

A serious drawback is that we only have information on the mid-plane; we do not know to what extent this plane is representative for the rest of the vessel. The comparison of the theoretical and experimental results will finally have to justify the assumptions.

From the analysis given in Sect. 3 we learn that an accurate theoretical prediction of the rotational velocity can be made provided μ, I and B_0 are accurately known and the effective Hall parameter β_{eff} and σ (the Hartmann number H) are roughly known. We take the coefficient of viscosity of neutral argon; Dymond [22] gives a value $\mu = 1.14 \times 10^{-4}$ kg m^{-1} sec^{-1} for argon at an (average) temperature of 2900 K. The average effective Hall parameter is determined in the following way: from the arc voltage/current plot at constant B the voltage difference ΔV beteeen cathode and anode without the cathode and anode falls can be determined. In case of $B = 0.13$ T (diffuse mode) this value is $\Delta V = 18.5 \pm 2$ V. This voltage difference is also an output of the theoretical calculation given in Sect. 3 provided σ, $\mu(H)$ and β_{eff} are known. On the other hand, the knowledge of σ, μ and ΔV leads to a value for β_{eff}. If we use the above mentioned values for μ and ΔV than insertion of the Spitzer conductivity for $T_e = 1.0$ and 2.5 eV (see Sect. 4.3) yields values for β_{eff} equal to 3 and 9, respectively. For these two values of β_{eff} the calculated velocity profiles are plotted in Figure 9. Because the degree of ionization is only a few percent, the neutral particle velocity may be considered to be equal to the overall fluid-velocity.

For $\beta_{\text{eff}}=9$ as well as $\beta_{\text{eff}}=3$ the calculated velocities agree rather well with the measured velocities of the neutral particles (Figure 9).

If we apply the same procedure to the contracted mode, then the measured "true" arc voltage $\Delta V=38$ V (see Table 1) and $\mu=1.5$ kg m^{-1} sec^{-1} lead to $\beta_{\text{eff}}=7$ and 23 for $T_e=1.2$ and 4.0 eV, respectively. The velocity profiles for these cases are given in Figure 10. As can be expected the theoretical velocity profiles lie somewhere in between the neutral and the ion data points.

Finally for the diffuse mode ($B=0.13$ T) the dependence of the rotational velocity on the current was measured. Within the accuracy of the measurements the velocity is linearly dependent on the current as can be expected from the analysis of Section 3.

4.6. Plasma Potential

For the diffuse mode the plasma potential is measured with an electrically floating probe from the wall inwards up to 2 cm. The measured values as well as the calculated profiles for $\beta_{\text{eff}}=3$ and 9 are given in Figure 11. The calculated voltage drop in radial direction is 3.75 V and 6.25 V respectively. The measured and calculated curves are taken coincident at 1.0 cm from the wall. Between the wall and 1 cm from the wall the measured curve is steeper than both the calculated ones. This is probably due to the fact that the conductivity close to the wall is lower than in the centre of the system. (Note that at the mid-plane the wall is floating.)

For the contracted discharge probe measurements were not performed due to the risk of melting the probe.

4.7. Pressure Distribution

The pressure distribution in the symmetry plane is measured by means of the pressure probe described in Sect. 2; it is moved radially inwards. This is done for various values of the magnetic field strength; see Figure 12a. In Fig. 12b the wall pressure is given as a (continuous) function of the magnetic field. When the discharge is in the diffuse mode ($B\leqq 0.17$ T) the radial pressure distribution becomes steeper with increasing magnetic field strength. At 0.17 T the discharge abruptly changes character; the wall pressure suddenly drops to a much lower value. However the radial pressure enhancement is still present. Note that in all measurements the pressure is kept constant at 1.0 torr in the two volumes behind the cathodes.

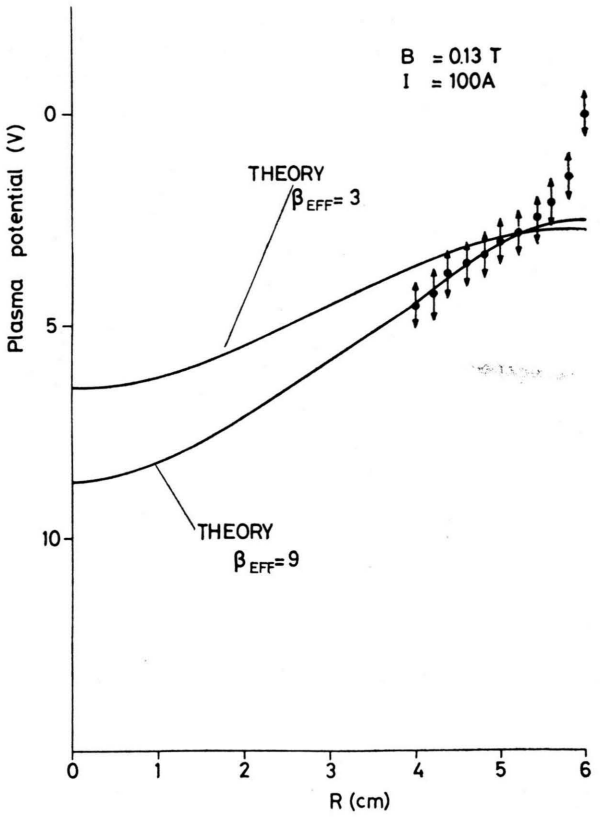

Fig. 11. The measured plasma potential (dots) and the theoretical one for $\beta_{\text{eff}}=3$ and 9 (solid curves) as a function of the radius. The theoretical and the measured curves are normalized at 1 cm from the wall. The magnetic field strength is 0.13 T, the arc current 100 A and the filling pressure 1 torr.

Because the other measurements are mainly concerned with the diffuse mode, we will compare theory and experiment for the (diffuse) case $B=0.13$ T.

According to Eq. (5) the pressure distribution is strongly dependent on the temperature and the temperature profile. Therefore, in the calculations we do not apply an average value for the temperature but use instead the temperature profile of Figure 7. Also v_θ, $\partial\varphi/\partial r$ and σ_H have to be known. Note that Eq. (3c) and consequently (5) is *not* coupled to (3a) and (3b), because the latter two equations do not contain the pressure p. This means that (5) can be solved independently i.e. either

theoretical or experimental values (profiles) for v_θ, $\partial\varphi/\partial r$ and σ_H can be inserted. For the Hall-conductivity σ_H one needs to know β_e and β_i. For determining β_e, the electron-ion and electron-atom collision frequencies and the ion and atom densities have to be known. β_i requires knowledge of the ion-neutral collision frequency and the neutral density. The ion and atom velocities can be determined from Figure 7.

For the electron temperature we take the measured value 1.0 eV. The ion (electron) density is given in Figure 8. The neutral density follows from Figures 7 and 12a. The pressure curve of Fig. 12a is extrapolated to the centre of the column. This of course only gives a rough indication of the neutral particle density in the centre. For the collision cross-section we take the following values: the Spitzer value for the electron-ion collisions, the value $Q_{en} = 4.0 \cdot 10^{-20}$ m^2 for the electron-argon atom cross-section (see Mitchner and Kruger [13] and Golden [23]). Because the ion-atom cross-section is mainly determined by the charge exchange process, we take $\bar{Q}_{in} = 6 \cdot 10^{-19}$ m^2 (Massey and Gilbody [24]). This charge exchange cross-section is assumed to be temperature independent in our limited temperature range. This leads to the following values for β_i and β_e: β_i decreases monotonically from 0.94 at the centre to 0.18 at 1 cm from the wall; β_e from 100 at the centre to 38 at 1 cm from the wall. Because $s \approx \beta_e \beta_i > 1$ [Eq. (8)] these numbers show that in the symmetry plane the major part of the radial current is carried by the ions.

As mentioned before the parallel conductivity σ is mainly determined by the electron-ion collisions. Only close to the wall the electron-atom collisions become more important (roughly 20% of the total number of collisions). σ varies from 1070 at the centre to 950 at 1 cm from the wall. Via Eq. (7) σ_H can be determined. σ_H is found to vary from 5.7 at the centre to 24 at 1 cm from the wall.

From β_i and β_e also the effective Hall coefficient β_{eff} can be determined via Equation (9). It appears that β_{eff} (and consequently $\sigma_\perp$) is practically constant between the centre and the wall. It varies between 12 and 14.

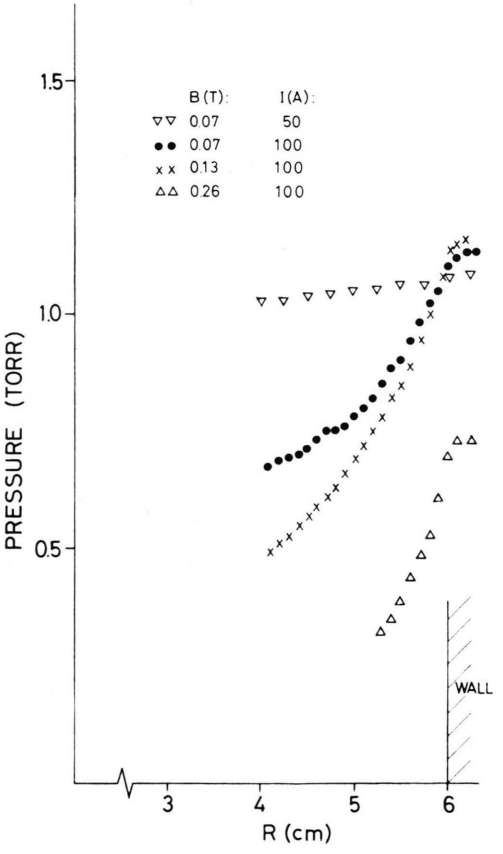

Fig. 12. a) The measured pressure distribution in radial direction for different currents and magnetic field strengths. The filling pressure is 1 torr. The pressures given for R > 6 cm are measured inside the channel in the wall in which the pressure probe is moved.

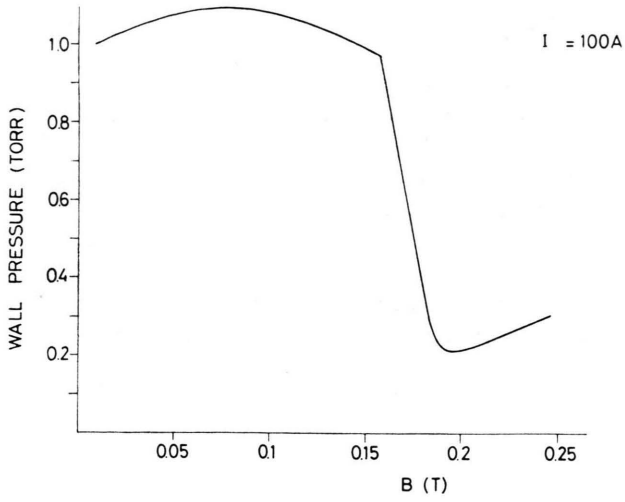

Fig. 12. b) The pressure at the wall as a function of magnetic field strength. At $B = 0.17$ T the discharge abruptly changes character. In the contracted mode ($B > 0.17$ T) the wall pressure is much lower than in the diffuse mode ($B \leqq 0.17$ T). The filling pressure is kept constant at 1 torr in the volumes behing the two cathodes.

For v_θ and $\partial\varphi/\partial r$ we take the theoretical values calculated for $\beta_{\text{eff}}=9$; see Figs. 9 and 11. Due to the fact that the experimental velocities are probably slightly too low for reasons mentioned in the beginning of Sect. 4.5, the $\beta_{\text{eff}}=9$ velocity curve probably is a good choice, also because, except in a thin layer close to the wall, the $\beta_{\text{eff}}=9$ potential curve is sufficiently close to the measured one.

An analysis of the two terms on the right-hand side of (5) now shows that the Hall term is small compared to the centrifugal term.

Numerical integration of Eq. (5) now gives the pressure as a function of radius (see Figure 13). The contribution due to the Hall term has a maximum value at the wall: approximately 5%. It is clear that the measured pressure rise from the centre to the wall is much larger than the calculated one; it also has a different shape.

The pressure enhancement is strongly dependent on the rotational velocities and the plasma temperature. To illustrate this Fig. 13 also shows the pressure distribution in case v_θ^2/T is twice as large and four times as large as in the experimental situation. However, the steep rise in the pressure close to the wall is not present in any of these cases. Equation (15) allows for a slope at the wall unequal to zero only if the velocity at the wall is non-zero. To illustrate this, the velocity profile required to generate a pressure distribution as given in Fig. 12a (0.13 T) is calculated and given in Fig. 9 (dashed line).

In view of the velocity and temperature measurements (Figs. 9 and 7) we do not believe that the dashed velocity profile (Fig. 9) is realistic. It requires too high a velocity and because exactly on the wall the velocity necessarily has to be zero it would lead to severe shear there. Therefore we doubt that Eq. (5) is very useful in predicting

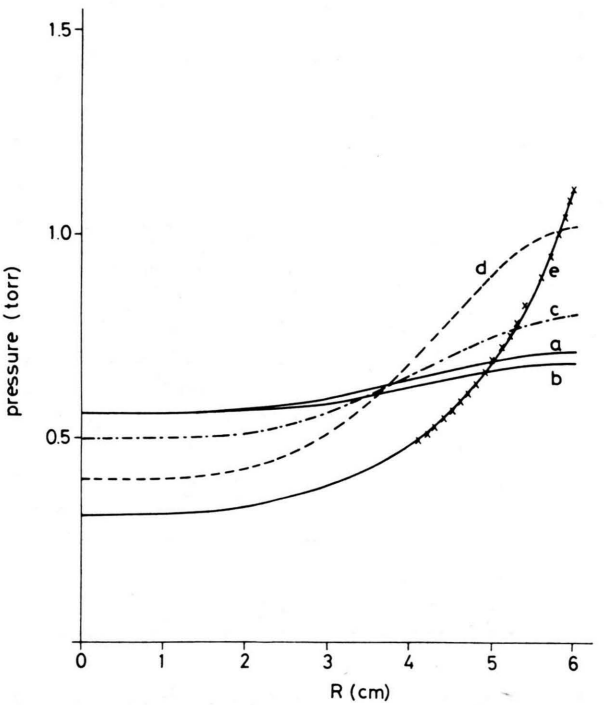

Fig. 13. Theoretical radial pressure profiles. The measured points are those obtained for $I=100$ A and $B=0.13$ T. a) and b): Calculated profiles for the experimental parameters according to equation (5), in case the Hall effect is absent and present, respectively, [second term on right-hand side of Eq. (5)]. c) and d): theoretical curves in case the quantity v^2/T is twice and four times as large as experimentally determined. The Hall effect is not taken into account. e) theoretical profile which is obtained when the dashed velocity profile of Fig. 9 is assumed to be valid. The temperature profile is taken to be that of Fig. 7; the Hall effect is not taken into account.

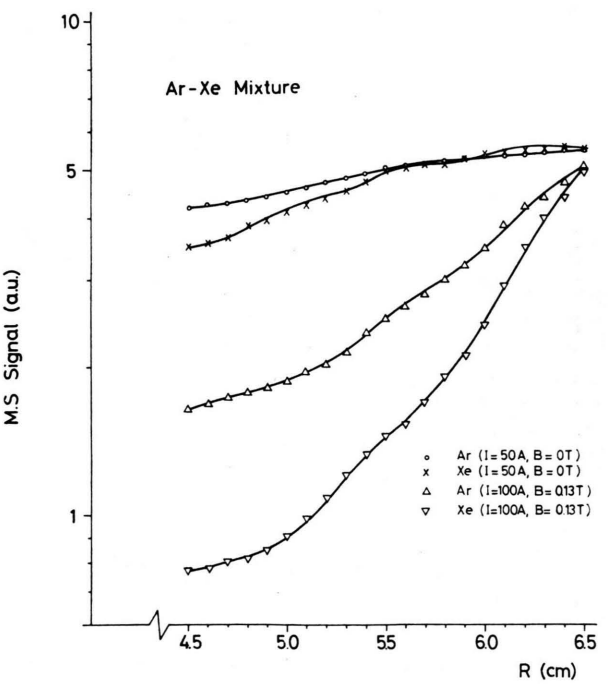

Fig. 14. Mass spectrometer measurements on argon and xenon in a discharge containing a mixture of these gases. A small flow of gas is continuously pumped from the vessel to the mass spectrometer. The points given for $R>6$ cm are measured inside the channel in the wall in which the probe is shifted. The heavy gas, Xe, shows the largest radial enhancement.

accurate pressure distributions. Possibly secondary flows in radial and axial direction have to be taken into account.

Finally measurements are done on a discharge containing a mixture of argon and xenon. Through a small hole in the pressure probe the gas is pumped to a mass spectrometer where the composition is determined; see Figure 14. It is clear that the partial pressure rise of the heavy component, is larger than that of the light one. So, indeed, centrifugal forces are separating species with different atomic mass. Now we can define a relative separation factor α (Cohen [25]) for argon and xenon for any set of two points in the system. If we take the two points located at the wall and 2 cm from the wall, we find $\alpha = 2.15$.

5. Conclusions

In the partially ionized rotating plasma experiment described in this paper the discharge can exist in two different modes. At the filling pressure of 1 torr the argon discharge changes abruptly from a diffuse into a more contracted state at a magnetic field strength of 0.17 T.

In the more diffuse state which is present at lower magnetic field strength the discharge fills the cylindrical vessel uniformly. The rotation of the particles leads to a pressure enhancement near the cylinder wall of about a factor two or three. The ions and neutrals have approximately the same maximum velocity (700 m/s). However, the radial positions of these velocity maxima do not coincide. At the symmetry plane of the device close to the wall the neutrals have a higher velocity than the ions. Consequently the neutrals can not be driven by the ions there. Probably via viscous forces they are driven by plasma particles rotating at a higher speed elsewhere in the machine. The theory developed by Klüber and Wilhelm and Hong for a homogeneous plasma, adapted to our experimental arrangement, predicts velocity- and potential profiles which are in good agreement with the measured ones. The calculated pressure enhancement, however, rather deviates from the measured one. In the symmetry plane the radial electrical current is carried mainly by the ions. In this diffuse mode the experimental results indicate that it is possible to separate argon en xenon. The maximum separation factor is 2.15. This value are still rather low. However, the device will be changed in such a way that this diffuse mode can also be maintained at higher magnetic fields. Consequently, the driving force will be larger which may have a favourable effect on the separation.

In the more contracted mode the wall pressure is much smaller than in the diffuse mode. However, the radial pressure enhancement at the wall is still present. There is a large velocity slip between ions and neutrals. The ions have a maximum velocity of 1900 m/s close to the axis of the experiment while the neutrals have a broad maximum of about 650 m/s. Strictly speaking, in this case the developed theory can not be applied since the plasma is not homogeneous. It predicts a velocity profile which lies in between the neutral and ion velocity profiles. For this mode an increase of magnetic field strength and/or discharge current will probably not lead to proportionally higher neutral particle velocities.

Appendix

In solving the boundary value problem mentioned in Sect. 3 (see Fig. 3) we restrict ourselves to the left hand side of the vessel i.e. $-c \leqq z \leqq 0$ and $0 \leqq r \leqq R_0$. Now, the potential φ and the azimuthal velocity v have to be determined from Eqs. (3a) and (3b) taking into account the following boundary conditions:

$$v(r,z) = 0 \quad \text{at} \quad z = -c \quad \text{and} \quad r = R_0\,, \tag{A.1}$$

$$\frac{\partial v(r,z)}{\partial z} = 0 \quad \text{at} \quad z = 0\,, \tag{A.2}$$

$$\frac{\partial \varphi(r,z)}{\partial z} = 0 \quad \text{at} \quad z = 0\,, \tag{A.3}$$

$$-\sigma \frac{\partial \varphi(r,z)}{\partial z} = I \frac{\delta(r - R_1)}{2\pi r} \quad \text{at} \quad z = -c\,, \tag{A.4}$$

$$-\sigma_\perp \frac{\partial \varphi(r,z)}{\partial r} = I \frac{\delta(z + c_0)}{2\pi R_0} \quad \text{at} \quad r = R_0\,. \tag{A.5}$$

This boundary value problem is essentially difficult to solve due to the fact that the boundary conditions (A.4) and (A.5) are located on different types of boundaries, namely one on the flat end wall of the cylinder and the other on the cylinder itself. We therefore split the problem into two parts. Because (3a) and (3b) are linear differential equations, solutions for different current paths can be added, provided the boundary conditions for the different current paths are matched (see Figure 15).

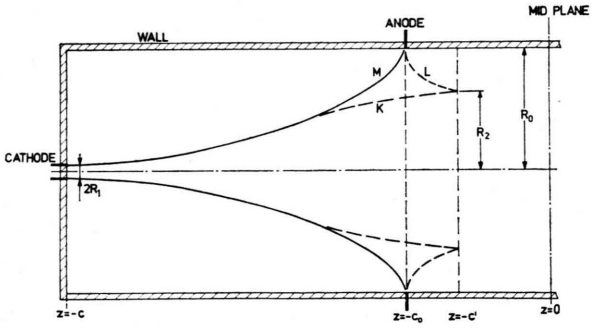

Fig. 15. Simplified scheme of the discharge used in the theoretical model. For explanations of the symbols see text.

First we solve the equation for the boundary conditions (A.1)—(A.4) and

$$-\sigma\frac{\partial\varphi(r,z)}{\partial r}=I\frac{\delta(r-R_2)}{2\pi r}\quad\text{at}\quad z=-c', \tag{A.6}$$

i.e. for current path K, and subsequently for the boundary conditions (A.1)—(A.3), (A.5) together with

$$-\sigma\frac{\partial\varphi(r,z)}{\partial r}=-I\frac{\delta(r-R_2)}{2\pi r}\quad\text{at}\quad z=-c', \tag{A.7}$$

(current path L).

Addition of these two solutions leads to the final solution of the problem for the desired boundary conditions (A.1)—(A.5) (current path M). Now, in the limiting case $c'\to c_0$ and $R_2\to R_0$ the influence of the second part of the solution (L) on the total solution (M) becomes vanishingly small. Consequently in that case one needs to solve the problem for the boundary conditions (A.1)—(A.4) and (A.6) with $R_2=R_0$.

We now introduce the following dimensionless coordinates and quantities (W & H, [9])

$$\varrho=r/R_0,\qquad 0\leqq\varrho\leqq 1,$$
$$\xi=z/C_0,\quad -1\leqq\xi\leqq 0, \tag{A.8}$$

$$\Phi(\varrho,\xi)=\varphi(r,z)/\varphi_0;$$
$$\varphi_0=I\,c/2\pi\,\sigma\,R_0^2, \tag{A.9}$$

$$V(\varrho,\xi)=v(r,z)/v_0;$$
$$v_0=\varphi_0/R_0\,B_0, \tag{A.10}$$

$$N=c/R_0, \tag{A.11}$$

$$M=(c/R_0)/[1+\beta_{\text{eff}}^2]^{1/2}, \tag{A.12}$$

$$H_\perp=H/[1+\beta_{\text{eff}}^2]^{1/2}. \tag{A.13}$$

Equation (3a) and (3b) now become:

$$\frac{1}{\varrho}\frac{\partial}{\partial\varrho}\left(\varrho\frac{\partial\Phi}{\partial\varrho}\right)+M^{-2}\frac{\partial^2\Phi}{\partial\xi^2}=\frac{1}{\varrho}\frac{\partial}{\partial\varrho}(\varrho\,V), \tag{A.14}$$

$$\frac{\partial}{\partial\varrho}\left\{\frac{1}{\varrho}\frac{\partial}{\partial\varrho}(\varrho\,V)\right\}+N^{-2}\frac{\partial^2V}{\partial\xi^2}-H_\perp{}^2\,V=-H_\perp{}^2\frac{\partial\Phi}{\partial\varrho}. \tag{A.15}$$

We again split the remaining part of the problem into two parts concerning the cylindrical volumes

A: $-1\leqq\xi\leqq-\xi_0$ $(-c\leqq z\leqq-c_0)$ and
B: $-\xi_0\leqq\xi\leqq 0$ $(-c_0\leqq z\leqq 0)$.

In that case on the common surface the solutions for the velocity and the potential have to be continuous.

For the solution of the problem in parts A and B we can generally write:

$$\Phi^A(\varrho,\xi)=-2\xi+\sum_{\nu=1}^{\infty}J_0(k_\nu\varrho)\,f_\nu{}^A(\xi), \tag{A.16a}$$

$$V^A(\varrho,\xi)=\sum_{\nu=1}^{\infty}J_1(k_\nu\varrho)\,g_\nu{}^A(\xi), \tag{A.16b}$$

$$\Phi^B(\varrho,\xi)=2\xi_0+\sum_{\nu=1}^{\infty}J_0(k_\nu\varrho)\,f_\nu{}^B(\xi), \tag{A.17a}$$

$$V^B(\varrho,\xi)=\sum_{\nu=1}^{\infty}J_1(k_\nu\varrho)\,g_\nu{}^B(\xi). \tag{A.17b}$$

J_0 and J_1 are the zeroth and first order Bessel functions, and k_ν is the ν-th zero point of the first order Bessel function. In terms of the dimensionless coordinates and quantities (A.8)—(A.13) the various boundary conditions of the volumes A and B become:

$$[V^{A,B}(\varrho,\xi)]_{\varrho=1}=\left[\frac{\partial\Phi^{A,B}(\varrho,\xi)}{\partial\xi}\right]_{\varrho=1}=0;$$
$$J_1(k)=0, \tag{A.18}$$
$$[V^A(\varrho,\xi)]_{\xi=-1}=\left[\frac{\partial V^B(\varrho,\xi)}{\partial\xi}\right]_{\xi=0}=\left[\frac{\partial\Phi^B(\varrho,\xi)}{\partial\xi}\right]_{\xi=0}=0$$

this gives

$$[g^A(\xi)]_{\xi=-1}=\left[\frac{\mathrm{d}g_\nu{}^B(\xi)}{\mathrm{d}\xi}\right]_{\xi=0}=\left[\frac{\mathrm{d}f_\nu{}^B(\xi)}{\mathrm{d}\xi}\right]_{\xi=0}=0,$$
$$\left[\frac{\partial\Phi^A(\varrho,\xi)}{\partial\xi}\right]_{\xi=-1}=\frac{-\delta(\varrho-\varrho_1)}{\varrho} \tag{A.19}$$
$$=-2-2\sum_{\nu=1}^{\infty}\frac{J_0(k_\nu\varrho_1)}{J_0{}^2(k_\nu)}J_0(k_\nu\varrho)$$

this gives

$$\left[\frac{\mathrm{d}f_\nu^A(\xi)}{\mathrm{d}\xi}\right]_{\xi=-1} = \frac{-2J_0(k_\nu \varrho_1)}{J_0^2(k_\nu)}. \tag{A.20}$$

In order to be able to solve the Eqs. (A.14) and (A.15) for both volumes A and B separately we need to know two boundary conditions on the common plane $\xi = -\xi_0$. For these we choose $\partial V/\partial\xi$ and $\partial\Phi/\partial\xi$. At the plane $\xi = -\xi_0$ we can express $\partial V/\partial\xi$ in an infinite series of first order Bessel functions in the following way:

$$\left[\frac{\partial V^{A,B}(\varrho,\xi)}{\partial\xi}\right]_{\xi=-\xi_0} = \sum_{\nu=1}^{\infty} a_\nu J_1(k_\nu \varrho);$$

this leads to

$$\left[\frac{\mathrm{d}g^{A,B}(\xi)}{\mathrm{d}\xi}\right]_{\xi=-\xi_0} = a_\nu. \tag{A.21}$$

Note that at $\xi = -\xi_0$, $\partial V/\partial\xi$ is a function of ϱ only. $\partial\Phi/\partial\xi$ can be expressed in the following way:

$$\left[\frac{\partial\Phi^A(\varrho,\xi)}{\partial\xi}\right]_{\xi=-\xi_0} = \frac{-\delta(\varrho-\varrho_2)}{\varrho} + h(\varrho); \tag{A.22a}$$

$$\left[\frac{\partial\Phi^B(\varrho,\xi)}{\partial\xi}\right]_{\xi=-\xi_0} = h(\varrho). \tag{A.22b}$$

In this case the radial δ-function $\delta(\varrho-\varrho_2)/\varrho$ ensures that the current flows to the anode ring at radius ϱ_2 (note that at the end of the calculation we take the limit $\varrho_2 \to 1$). The function $h(\varrho)$ allows a part of the current to flow across the plane $\xi = -\xi_0$ before going to the anode ring. Any current entering volume B through this plane should of course also leave this volume through the same plane. This condition can be expressed in the following way: $h(\varrho)$ should be chosen such that

$$-\int_0^1 \left[\frac{\partial\Phi^A(\varrho,\xi)}{\partial\xi}\right]_{\xi=-\xi_0} \varrho\,\mathrm{d}\varrho = 1 \quad \text{and}$$

$$-\int_0^1 \left[\frac{\partial\Phi^B(\varrho,\xi)}{\partial\xi}\right]_{\xi=-\xi_0} \varrho\,\mathrm{d}\varrho = 0 \quad \text{or}$$

$$\int_0^1 h(\varrho)\,\varrho\,\mathrm{d}\varrho = 0.$$

If we choose

$$h(\varrho) = \sum_{\nu=1}^{\infty} b_\nu J_0(k_\nu \varrho), \tag{A.23}$$

this condition is fulfilled. Now:

$$\left[\frac{\mathrm{d}f_\nu^A(\xi)}{\mathrm{d}\xi}\right]_{\xi=-\xi_0} = \frac{-2J_0(k_\nu \varrho_2)}{J_0^2(k_\nu)} + b_\nu, \tag{A.24a}$$

$$\left[\frac{\mathrm{d}f_\nu^B(\xi)}{\mathrm{d}\xi}\right]_{\xi=-\xi_0} = b_\nu. \tag{A.24b}$$

If we substitute the general solutions (A.16) and (A.17) into the differential equations (A.14) and (A.15), and take into account the boundary conditions (A.18)—(A.24) this yields the functions $f_\nu(\xi)$ and $g_\nu(\xi)$ expressed in the parameters a_ν and b_ν. This leads to solutions for $\Phi^A(\varrho,\xi)$, $V^A(\varrho,\xi)$ and for $\Phi^B(\varrho,\xi)$, $V^B(\varrho,\xi)$ again expressed in terms of a_ν and b_ν.

Putting

$$[\Phi^A(\varrho,\xi)]_{\xi=-\xi_0} = [\Phi^B(\varrho,\xi)]_{\xi=-\xi_0}$$

and

$$[V^A(\varrho,\xi)]_{\xi=-\xi_0} = [V^B(\varrho,\xi)]_{\xi=-\xi_0}$$

one can eliminate a_ν and b_ν for each term ν of the infinite series separately. This means that the functions $f_\nu^{A,B}(\xi)$ and $g_\nu^{A,B}(\xi)$ and consequently $\Phi^{A,B}(\varrho,\xi)$ and $V^{A,B}(\varrho,\xi)$ are fully known.

We will now give the formal solution. Note that the first few of the expressions are already given in W & H. (A.16) and (A.17) are the final solutions in which

$$f_\nu^{A,B}(\xi) = K_{1\nu} C_{1\nu}^{A,B} \frac{\sinh\omega_{1\nu}\xi}{\sinh\omega_{1\nu}} + K_{1\nu} D_{1\nu}^{A,B} \frac{\cosh\omega_{1\nu}\xi}{\cosh\omega_{1\nu}} + K_{2\nu} C_{2\nu}^{A,B} \frac{\sinh\omega_{2\nu}\xi}{\sinh\omega_{2\nu}} + K_{2\nu} D_{2\nu}^{A,B} \frac{\cosh\omega_{2\nu}\xi}{\cosh\omega_{2\nu}}, \tag{A.25a}$$

$$g_\nu^{A,B}(\xi) = C_{1\nu}^{A,B} \frac{\sinh\omega_{1\nu}\xi}{\sinh\omega_{1\nu}} + D_{1\nu}^{A,B} \frac{\cosh\omega_{1\nu}\xi}{\cosh\omega_{1\nu}} + C_{2\nu}^{A,B} \frac{\sinh\omega_{2\nu}\xi}{\sinh\omega_{2\nu}} + D_{2\nu}^{A,B} \frac{\cosh\omega_{2\nu}\xi}{\cosh\omega_{2\nu}}, \tag{A.25b}$$

in which

$$\omega_{1\nu,2\nu} = [\tfrac{1}{2}([k_\nu^2(M^2+N^2) + N^2 H_\perp^2] \pm \{[k_\nu^2(M^2+N^2) + N^2 H_\perp^2]^2 - 4k_\nu^4 M^2 N^2\}^{1/2})]^{1/2}. \tag{A.26}$$

From now on we omit all indices ν; all the following formulae hold for each term ν of the infinite series.

$$K_{1,2} = \frac{k M^2}{(\omega_{1,2}^2 - k^2 M^2)}, \tag{A.27}$$

$$
\begin{aligned}
C^A_{1,2} &= F_{1,2} - H_{1,2}\,a \pm O_{1,2}\,b\,,\\
D^A_{1,2} &= G_{1,2} - L_{1,2}\,a \mp X_{1,2}\,b\,,\\
C^B_{1,2} &= 0\,,\\
D^B_{1,2} &= Y_{1,2}\,a \mp Z_{1,2}\,b\,.
\end{aligned}
\tag{A.28}
$$

Before we define the various quantities in these equations we first make the following substitutions:

$$
R_{1,2} = \omega_{1,2}\frac{\sinh\omega_{1,2}\xi_0}{\cosh\omega_{1,2}};\quad S_{1,2} = \omega_{1,2}\frac{\cosh\omega_{1,2}\xi_0}{\sinh\omega_{1,2}},
$$

$$
T_{1,2} = \frac{\cosh\omega_{1,2}\xi_0}{\cosh\omega_{1,2}};\quad U_{1,2} = \frac{\sinh\omega_{1,2}\xi_0}{\sinh\omega_{1,2}},
$$

$$
P_{1,2} = \frac{(K_{2,1}\,T_{1,2} - K_{1,2}\,T_{2,1})\,S_{1,2}}{K_{2,1}\,T_{1,2}(T_{2,1} - U_{2,1})} - \frac{(S_{1,2} - S_{2,1})\,R_{2,1}}{U_{2,1}(S_{2,1} - R_{2,1})},
$$

$$
Q_{1,2} = \frac{(K_{1,2}\,T_{2,1} - K_{2,1}\,U_{1,2})\,R_{1,2}}{K_{2,1}\,U_{1,2}(T_{2,1} - U_{2,1})} - \frac{(S_{2,1} - R_{1,2})\,R_{2,1}}{U_{2,1}(S_{2,1} - R_{2,1})},
$$

$$
V_{1,2} = \frac{2J_0(k\varrho_1)}{J_0^2(k)}\,\frac{T_{1,2}}{K_{1,2}(T_{1,2} - U_{1,2})};
$$

$$
W = \frac{2J_0(k\varrho_2)}{J_0^2(k)(K_1 - K_2)}.
$$

$$
F_{1,2} = \frac{R_{1,2}\,V_{2,1} \mp W\,Q_{1,2}}{R_{1,2}\,P_{1,2} + S_{1,2}\,Q_{1,2}};
$$

$$
G_{1,2} = \frac{S_{1,2}\,V_{1,2} \pm W\,P_{1,2}}{R_{1,2}\,P_{1,2} + S_{1,2}\,Q_{1,2}};
$$

$$
H_{1,2} = \frac{1}{R_{1,2}\,P_{1,2} + S_{1,2}\,Q_{1,2}} \cdot \left[\frac{R_1 R_2}{(S_{2,1} - R_{2,1})} \pm \frac{K_{2,1}\,Q_{1,2}}{(K_1 - K_2)} - \frac{R_{1,2}}{(T_{2,1} - U_{2,1})}\right];
$$

$$
L_{1,2} = \frac{1}{R_{1,2}\,P_{1,2} + S_{1,2}\,Q_{1,2}} \cdot \left[\frac{S_{1,2}\,R_{2,1}}{(S_{2,1} - R_{2,1})} \mp \frac{K_{2,1}\,P_{1,2}}{(K_1 - K_2)} - \frac{S_{1,2}}{(T_{2,1} - U_{2,1})}\right],
$$

$$
O_{1,2} = \frac{Q_{1,2}}{(K_1 - K_2)(R_{1,2}\,P_{1,2} + S_{1,2}\,Q_{1,2})};
$$

$$
X_{1,2} = \frac{P_{1,2}}{(K_1 - K_2)(R_{1,2}\,P_{1,2} + S_{1,2}\,Q_{1,2})},
$$

$$
Y_{1,2} = \frac{\pm K_{2,1}}{(K_1 - K_2)\,R_{1,2}};\quad Z_{1,2} = \frac{1}{(K_1 - K_2)\,R_{1,2}},
$$

$$
\begin{aligned}
\alpha_{1,2} &= T_{1,2}\,G_{1,2} - U_{1,2}\,F_{1,2}\,,\\
\beta_{1,2} &= U_{1,2}\,Q_{1,2} + T_{1,2}(X_{1,2} - Z_{1,2})\,,\\
\mu_{1,2} &= -\,U_{1,2}\,H_{1,2} + T_{1,2}(Y_{1,2} + L_{1,2})\,.
\end{aligned}
$$

This finally leads to the two quantities a_ν and b_ν which came about in (A.28):

$$
a_\nu = \frac{\alpha_1\beta_2 + \alpha_2\beta_1}{\mu_1\beta_2 + \mu_2\beta_1};\quad b_\nu = \frac{\alpha_1\mu_2 - \alpha_2\mu_1}{\mu_1\beta_2 + \mu_2\beta_1}.
$$

Acknowledgement

The authors wish to thank R. Groenewegen for skilful technical assistance.

This work was supported by the Ministry for Science and performed at the F.O.M.-Institute for Atomic and Molecular Physics in Amsterdam, the Netherlands.

[1] B. Bonnevier, Plasma Phys. **13**, 763 (1971). B. Bonnevier, Arkiv Fysik **33**, 15 (1966).
[2] B. W. James and S. W. Simpson, Plasma Phys. **18**, 289 (1976).
[3] N. Nathrath, H. Kress, J. McClure, G. Muck, and M. Simon, Proc. of the Int. Conf. on Uranium Isotope Separation (London), 9 (1975).
[4] A. Morozov, Plasma Acceleration Conference, Minsk (USSR), May 1976.
[5] N. Lehnert, Physica Scripta **7**, 102 (1973).
[6] F. Boeschoten, Proc. of the Int. Conf. on Uranium Isotope Separation (London), 11 (1975).
[7] J. J. McClure and N. Nathrath, XIIIth ICPIC, Berlin (1977).
[8] O. Klüber, Z. Naturforsch. **25a**, 1583 (1970).
[9] H. E. Wilhelm and S. H. Hong, J. Appl. Phys. **48**, 2 (1977).
[10] B. W. James and S. W. Simpson, Plasma Phys. **20**, 759 (1978).
[11] R. W. P. McWhirter, Plasma Diagn. Techn., R. H. Huddlestone, and S. L. Leonard, Los Angeles 1965.
[12] F. F. Chen, Plasma Diagn. Techn., R. H. Huddlestone and S. L. Leonard, Los Angeles 1965.
[13] M. Mitchner and C. H. Kruger, Partially Ionized Gases, Wiley, New York, London, Sydney Toronto 1973.
[14] P. Janssen, Eindhoven, to be published.
[15] G. N. Gerasimov, Opt. Spectrosc. (USSR), **43**, 209 (1977).
[16] K. N. Ulyanov, Sov. Phys. Tech. Phys. **18**, 3 (1973).
[17] V. Yu. Baranov and K. N. Ulyanov, Sov. Phys. Tech. Phys., **14**, 2 (1969).
[18] W. L. Wiese, Plasma Diagn. Techn., R. H. Huddlestone and S. L. Leonard, Los Angeles, 1965.
[19] H. Kress, Munich, private communication.
[20] B. F. M. Pots, B. van der Sijde, and D. C. Schram, Physica **94C**, 369 (1978).

[21] J. T. Davies and J. M. Vaughan, Astrophys. J. **137**, 1302 (1963).
[22] J. H. Dymond, J. Phys. B., Atom. Molec. Phys. **4**, 621 (1971).
[23] D. E. Golden, Phys. Rev. **151**, 48 (1966).
[24] H. S. W. Massey and H. B. Gilbody, Electronic and ionic impact phenomena, Vol. IV, Oxford (1974), p. 2772.
[25] K. Cohen, The Theory of Isotope Separation as Applied to the Large Scale Production of U^{235}, McGraw-Hill, New York 1951.